Young's modulus and thermal expansion of tensioned graphene membranes

Isaac R. Storch, Roberto De Alba, Vivekananda P. Adiga, T. S. Abhilash, Robert A. Barton, Harold G. Craighead, Jeevak M. Parpia, and Paul L. McEuen

Phys. Rev. B **98**, 085408 — Published 6 August 2018

DOI: 10.1103/PhysRevB.98.085408

Young's Modulus and Thermal Expansion of Tensioned Graphene Membranes

Isaac R. Storch,[*,†] Roberto De Alba,[†] Vivekananda P. Adiga,[‡] T. S. Abhilash,[†] Robert A. Barton,[‡] Harold G. Craighead,[‡] Jeevak M. Parpia,[†] and Paul L. McEuen[*,†,¶]

†*Department of Physics, Cornell University, Ithaca, New York, 14853, United States*

‡*School of Applied and Engineering Physics, Cornell University, Ithaca, New York, 14853, United States*

¶*Kavli Institute at Cornell for Nanoscale Science, Cornell University, Ithaca, New York, 14853, United States*

E-mail: irs9@cornell.edu; plm23@cornell.edu

Abstract

Tensioned graphene membranes are of interest both for fundamental physics and for applications ranging from water filtration to nanomechanical resonators. It is generally assumed that these membranes have a stretching modulus of about 340 N/m and a negative, temperature-independent thermal expansion coefficient due to transverse phonon modes. In this paper, we study the Young's modulus and thermal expansion of graphene as functions of temperature using laser interferometry to detect the static displacement of the membrane in a cryostat. Surprisingly, we find the modulus decreases strongly with increasing temperature, which leads to a positive temperature-dependent thermal expansion coefficient. We show that the thermally-rippled membrane theory is not consistent with our data, while the effects of surface contaminants typically present

on these membranes may explain the observed behavior. Our experiments undermine long-standing assumptions about tensioned 2D membranes, but are consistent with puzzling behaviors observed in previous experiments on graphene resonators.

Keywords

graphene, nano-electro-mechanical systems, Young's modulus, thermal expansion, nonlinear elasticity

Graphene is the ultimate limit of a 2D material, and it has been the subject of intense study since its isolation on a silicon substrate in 2004[1] and as a free-standing membrane in 2007.[2] It became known as the world's thinnest and strongest material, following an experiment that used an atomic force microscope (AFM) to stretch a suspended graphene sheet.[3] This experiment yielded the most commonly referenced value for the Young's modulus, 340 N/m, which is in agreement with atomistic theory. However, several preceding and subsequent experiments have given values ranging from 55-380 N/m for both exfoliated and chemical vapor deposited (CVD) graphene.[4–9] (For recent reviews, see Refs. 6 and 7) Understanding the mechanical properties of graphene, such as the Young's modulus, is important not only for studying fundamental membrane physics, but also because graphene is a promising material for nano-electromechanical systems (NEMS).[2] Advantages include high electrical conductivity, low mass, and high mechanical strength.[10] Several potential applications of graphene resonators have been demonstrated, such as mass and force sensing,[11] optomechanics,[13] and tunable radio frequency (RF) electronics.[14] Analysis of such experiments typically assumes a modulus of 340 N/m (despite the disagreement in the literature) and a negative thermal expansion coefficient (TEC). However, a number of unusual behaviors have been observed, most notably that the tension in a graphene membrane typically increases with decreasing temperature.[11,15] This is in direct contrast to expectations based on a negative TEC and clamped boundary conditions. Theory and numerical simulations have predicted a negative TEC in both un-tensioned and tensioned membranes, making

the argument that transverse thermal phonon modes cause the membrane to contract.[16] A number of experiments have given indirect support to this claim,[11,15,17,18] but no definitive experiments have yet been performed.

In this paper, we develop an optical technique for directly measuring the Young's modulus and the thermal expansion coefficient of a tensioned graphene membrane. This is done by applying an electrostatic force to the membrane and measuring its displacement. We use this technique to obtain force-distance curves over a wide range of temperatures, and find that the data is well fit by a model with linear and cubic terms ($F = c_1 z + c_3 z^3$). These measured parameters can be used to infer the tension and the added strain in the membrane. By interpreting the coefficient of the cubic term in the context of standard elastic theory[19,20] we get a measure of the 2D Young's modulus in the low strain regime. We find that the modulus is softer than expected at room temperature, but stiffens significantly as temperature decreases, approaching the theoretical value of 340 N/m. Recent work by Nicholl *et al.* has found similar results.[21] Furthermore, we find that the thermal expansion coefficient is positive and has a strong dependence on temperature and tension, which contradicts the established literature. Using a simple model, we show that this result follows directly from the temperature dependence of the Young's modulus. Finally, we propose that the softened modulus, its temperature dependence, and thus the effectively positive TEC can all be explained by the interaction between the graphene and surface contaminants. Our conclusions are relevant for graphene that has come into contact with any organic polymers during device fabrication, such as PMMA or photoresist, and may not apply to dry-transferred graphene that has had no additional processing.

Figure 1 shows schematics of the device geometries and experimental setups. A given device consists of an electrically contacted, nearly fully clamped, circular sheet of graphene suspended above a parallel metal electrode (i.e. the "gate"), which is used to apply a uniform electrostatic force. The devices are made by transferring single-layer graphene grown by chemical vapor deposition (CVD) onto pre-fabricated substrates using standard proce-

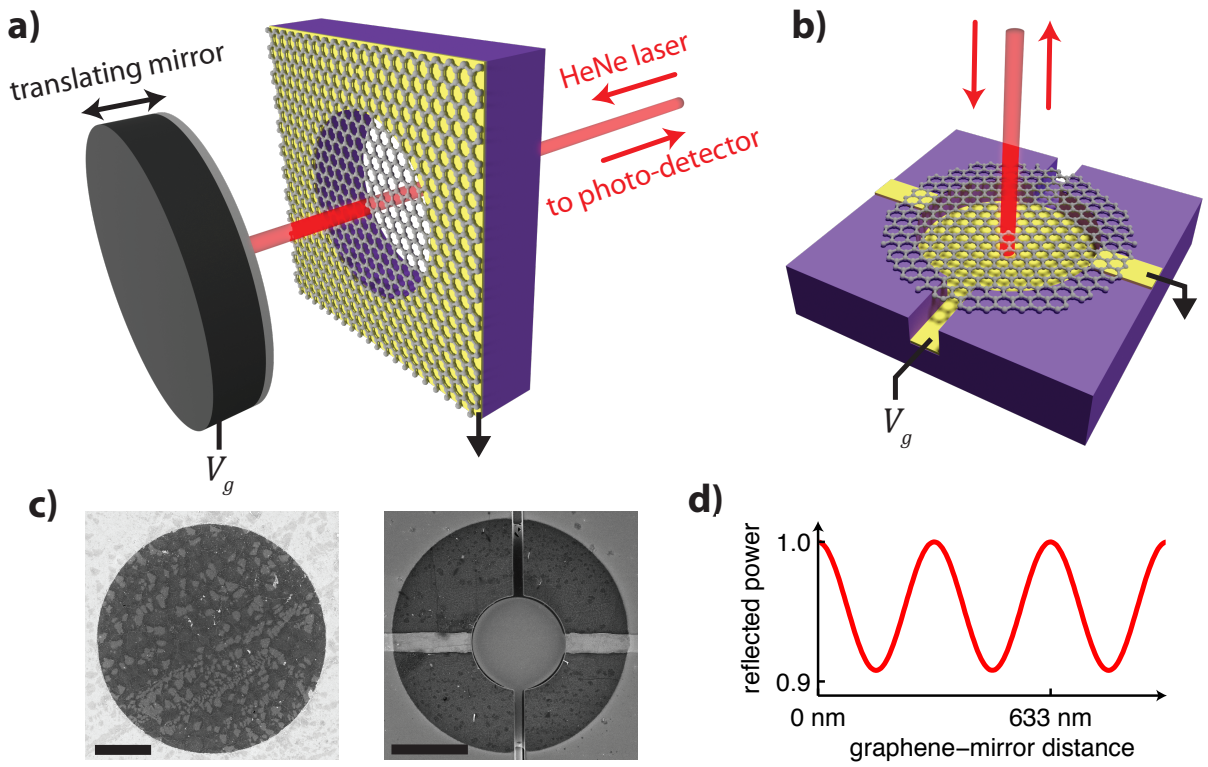

Figure 1: Devices and experimental setup. A focused laser beam is incident onto the sample and the intensity of the reflected light is measured by a photodiode. (a) Schematic of a through-hole graphene drum and the moving-mirror setup. A global gate voltage is applied to the mirror, while the sample is grounded. This setup allows for independently varying the distance between the graphene membrane and the back plane. (b) Schematic of a graphene device integrated with local electrodes on a substrate. The close proximity between the gate and graphene allow higher electrostatic forces to be applied. (c) Scanning electron micrographs (SEM) of the devices depicted in (a) and (b). Scale bars are each 10 µm. In the left image (a through-hole device), the large dark circle is the suspended graphene. In the right image (an integrated device), the large dark circle is the graphene supported by the silicon substrate, and the smaller circle in the center is the suspended graphene with the gate electrode behind it. (d) Illustration showing how the expected reflected laser power changes with graphene-mirror distance.

dures.[22] For this experiment, we use two different types of substrates: a 60 µm thick silicon substrate with holes etched all the way through for making "through-hole" devices (Fig. 1a), and a trench etched in silicon dioxide with local source, drain, and gate electrodes for making "integrated" devices (Fig. 1b).[13] One advantage of the through-hole device design is that very large graphene drums can be suspended, which is important for resonator applications, as the quality factor (Q) has been observed to increase linearly with radius.[23]

In order to select devices for our measurements, we examine the scanning electron micrographs (SEM) and make sure there are no tears or excessive amounts of visible contamination. Some level of contamination is present on most devices, and there is significant variation between fabrication runs. The two images shown in Fig. 1c are typical examples of devices used for measurement. The lighter patches on the through-hole device (the left image) and the darker patches on the integrated device (the right image) are bilayer graphene, which occurs at nucleation sites during CVD growth. The bright specks are large pieces of dirt that are scattered across every sample. Where possible, we select devices that do not have these large pieces of dirt on the suspended region of graphene, such as in the right image of Fig. 1c. It is important to note that the type of contamination that is relevant for our conclusions is a thin, inhomogeneous polymer coating, which would not be visible in these SEM images.

To clean these devices, we use standard procedures from the graphene resonator literature. The through-hole devices are annealed in a furnace using forming gas, as described in Ref. 24. However, furnace annealing consistently destroys the suspended region of graphene on the integrated devices, and so we current anneal them in vacuum instead. Current annealing has been shown to remove mass[11] and increase mobility.[25] Excessive annealing will cause damage to the graphene, and so we current anneal until the source-drain resistance is minimized (usually $\sim$10 kΩ) and the optically-measured resonance amplitude is maximized. The best way to quantify the efficacy of annealing is with transmission electron microscopy (TEM),[26] but unfortunately, we cannot use this technique on the integrated devices because

the substrate is too thick. However, the results from our optical measurements will show that current annealing is in practice not fully effective at removing residue, which agrees with Ref. 26.

Our experimental setup is similar to previous graphene resonator experiments,[2] in which membrane motion is detected through optical interference. The devices are mounted inside a vacuum chamber where the pressure is less than 10^{-6} Torr. A focused laser beam is incident on the device and reflected light is directed to a photodiode, whose DC and AC voltages are measured by a multimeter and network analyzer, respectively. The laser power is chosen to be low enough such that changes in laser power do not cause sufficient heating to shift the tension noticeably, as measured by the resonant frequency. The maximal change in temperature in the graphene due to laser heating is given by $\Delta T = \frac{2aP}{\pi\kappa t}$, where P is the incident laser power, and a, κ, and t are the absorption, thermal conductivity, and thickness of a graphene sheet.[13] The typical laser power used for detection is $\sim$100 µW, which results in $\sim$1 K heating of the graphene membrane.

Motion of the graphene is driven capacitively by applying a gate voltage. In the past, changes in the reflectance had been used to detect small displacements of high-frequency resonant devices,[2] but here we show that it can also be used to accurately measure static deflections. Similar measurements have also been done using optical profilometry[21,27] and scanning electron microscopy.[28]

The optical system is modeled as follows. Interference between the incident laser light and the light reflected off of the gate electrode behind the graphene creates a standing wave in the optical intensity. The graphene can be approximated as an infinitely thin absorbing interface.[13] This assumption is valid because the membrane thickness (0.34 nm) is much smaller than the wavelength of incident light (λ = 633 nm), and because the optical absorption a of graphene is 2.3%, while its reflectance is only 0.013%.[29] The optical intensity as a function of distance away from the reflecting back plane is $I(z) = 4I_0 \sin^2(2\pi z/\lambda)$, where I_0 is the intensity of the incident light. Hence, the overall reflectance is given by

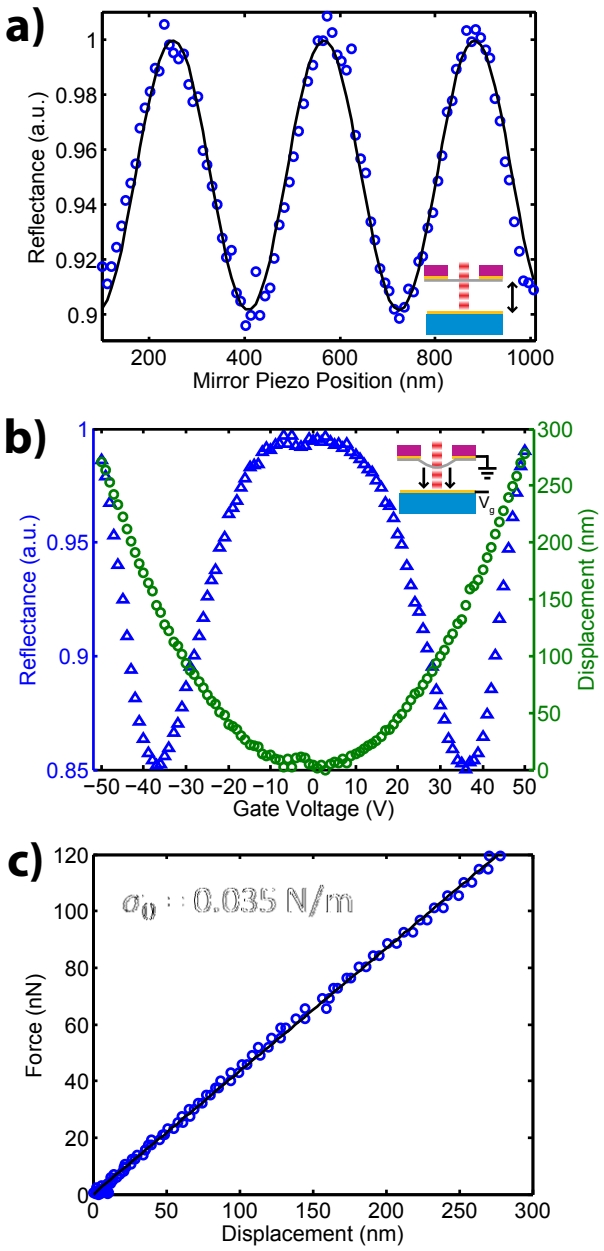

Figure 2: Data from a 21 µm radius through-hole graphene device in the moving-mirror setup. (a) Normalized intensity of the reflected light as a function of mirror position, obtained by measuring the DC voltage from the photodiode. The gap distance when zero voltage is applied to the mirror piezo is about 10 µm. (b) Total reflectance measured during a gate voltage sweep (blue triangles), and the same data converted to displacement versus gate voltage (green circles), using the change in reflectance during a piezo scan (not presented here) as a calibration. (c) Force-distance curve calculated from the gate voltage, assuming a parallel plate capacitor force. A linear fit to the data gives an initial tension $\sigma_0 = 0.035$ N/m.

$R(z) = 1 - 4a\sin^2(2\pi z/\lambda)$, which has a periodicity of $\lambda/2$. Note that the presence of a 1-2 nm layer of PMMA contamination on the surface would have a negligible effect on the interference profile because it is small compared to the wavelength of the laser.

The reflectance change with graphene position can be measured directly using the through-hole devices, which are mounted in a custom-built setup with the graphene parallel to a dielectric mirror attached to a piezo stepper (Fig. 1a).[24] By applying a voltage to the piezo, the distance between the graphene and the back plane can be varied. Figure 2a shows the measured reflectance as a function of mirror position. The data follows a sinusoidal pattern with a periodicity of $\sim$300 nm and an amplitude of $\sim$9%, in agreement with the equation above.

As Fig. 2a shows, there is a unique mapping from reflectance to displacement, as long as we know the maximum and minimum reflectance and which period the graphene is in. For the data in Fig. 2b, the distance between the graphene and the mirror is fixed, but the gate voltage is varied. Using the maximum and minimum reflectance obtained from a prior mirror piezo scan (not presented here), the reflectance (blue triangles) is converted into displacement (green circles). Note that the overall change in reflectance is about 50% larger than in Fig. 2a, which is most likely due to the presence of bilayer patches under the laser spot. Bilayer graphene has twice the absorption of single layer graphene, and judging by the SEM image in Fig. 1c, these patches are quite numerous on this device.

Assuming a parallel plate capacitor force $F = \frac{1}{2}\frac{\partial C}{\partial z}V_g^2$, where C is the capacitance and V_g is the gate voltage, the data in Fig. 2b can be plotted as force versus displacement (Fig. 2c). For a clamped circular membrane under uniform load, the force-distance curve has a linear term that is related to the initial tension σ_0,[30] and a cubic term that is related to the 2D Young's modulus E:[20]

$$F = 4\pi\sigma_0 z + \pi\frac{E}{g^3}\frac{z^3}{R^2} \tag{1}$$

where $g = 0.72 - 0.17\nu - 0.15\nu^2 = 0.69$ and $\nu = 0.15$ is the Poisson ratio for graphene.[31] The data in Fig. 2c is linear because the force is not large enough to resolve the cubic term.

A linear fit gives an initial tension of $\sigma_0 = 0.035$ N/m, which is in agreement with previous resonance-based measurements of suspended graphene.[11] Optomechanical forces could factor into Eq. 1, but we estimate these to be small: photothermal effects would change the tension by at most 0.002 N/m, and the force from radiation pressure would be at most 2×10^{-16}N (See Eqs. 4.9 and 4.18 in Ref. 12).

In order to access the cubic term of Eq. 1, and thereby measure the Young's modulus, much larger forces must be applied. This is not possible with the through-hole devices, as the minimum graphene-mirror distance is limited to ∼10 µm. However, larger forces are possible with the integrated device design (Fig. 1b), where the graphene-gate distance is ∼1.4 µm. One of the critical assumptions that goes into Eq. 1 is that the displacement of the membrane is small enough, relative to the gap distance, such that the parallel plate capacitor force does not change significantly with displacement. In this experiment, the maximum displacement is ∼300 nm, and so this assumption is valid for the through-hole devices, but it is arguably the case for the integrated devices. However, to the best of our knowledge, there is no approximation that will produce an analytic force-distance curve in the large displacement regime (See Sections 2.1.3 and 2.3 from Ref. 12 for additional discussion). For this work, we assume that Eq. 1 is a valid starting point; however, we suggest that future theoretical work should be done to investigate the potential effect that large displacements can have on the force-distance curve and modulus measurement.

Measurements of these devices were performed in a flow cryostat equipped with an optical window, where a continuous flow of liquid nitrogen and a temperature controller were used to vary the temperature. Note that the distance calibration requires pulling the graphene by at least $\lambda/4 \approx 160$ nm, which can only be done with the right combination of membrane diameter, tension, gap distance, and gate voltage. Figure 3a shows force-distance curves taken at two different temperatures. The data is well fit by Eq. 1, with the cubic dependence at high gate voltage (giving a large displacement) very clear on a log-log scale (Fig. 3a Inset). The Young's modulus at room temperature is 51 N/m and increases to 200 N/m at 78 K,

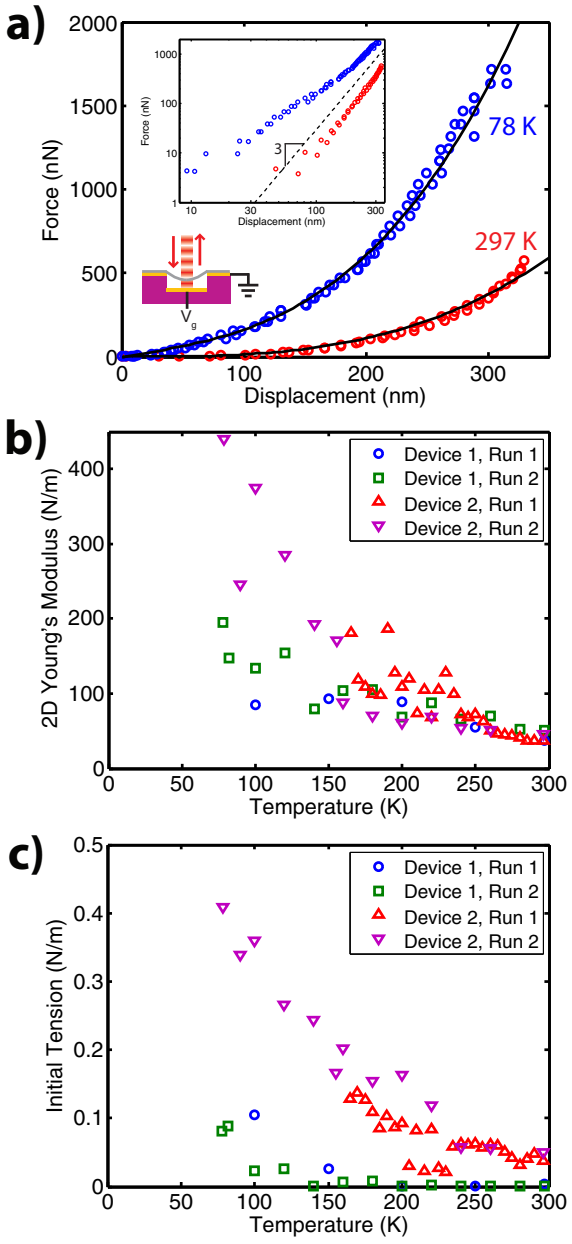

Figure 3: Data from two electrically integrated graphene devices in the cryostat. Device 1 has a 6.2 µm radius, Device 2 has a 5.2 µm radius, and the distance between the graphene and the gate is 1.4 µm for both devices. (a) Force-distance curves for Device 1 at two different temperatures, obtained by converting the change in reflectance to a displacement. The solid lines are fits of Eq. 1 to the data. The 2D Young's modulus from each fit is 51 N/m at 297 K and 200 N/m at 78 K. Inset: The same data plotted on a log-log scale, illustrating that the force-distance curve is strongly cubic at high gate voltage. (b,c) The Young's modulus (b) and initial tension (c) as a function of temperature for two different cool-down runs on each of these devices, inferred from force-distance curves like those shown in (a).

as indicated by the increase in the cubic term.

The temperature dependence of the modulus is plotted in Fig. 3b for two different cool-down runs on two different devices. Even though there is significant spread in the data, the modulus clearly increases with decreasing temperature. Figure 3c shows the initial tension inferred from the linear term in Eq. 1. In general, we find that the initial tension is often time-dependent, with sudden jumps triggered by changes in temperature or gate voltage. Both devices show an increasing initial tension with decreasing temperature, although for Device 1 the initial tension becomes large enough to be measured only at the lowest temperatures. The smaller changes in the modulus and initial tension when the temperature is cycled could be from adsorption and desorption of molecules on the surface, static ripples shifting, or delamination from the side walls. This can dramatically shift the initial tension in the membrane, but leaves the modulus relatively unaffected.

The thermal expansion coefficient of graphene at a fixed tension can be inferred by reframing the force-distance data in terms of stress and strain. For a tensioned circular drum under a uniform external force, the total tension and induced strain can be approximated by $\sigma \approx \frac{F}{4\pi z}$ and $\epsilon \approx \frac{2z^2}{3R^2}$, respectively.[21] Hence, we have three measured quantities that describe the system (stress, strain, and temperature), and two material properties that we are interested in (Young's modulus and thermal expansion coefficient). Figure 4a shows the stress-strain curves for the first cool-down run of Device 2, which are well-approximated by linear fits. The slopes of these lines are equal to the Young's modulus, which clearly increases with decreasing temperature. Finding the intersection between the linear fits and a constant stress yields the strain versus temperature curves in Figure 4b, which have been smoothed using a square window. For clarity, the data corresponding to $\sigma = 0.2$ N/m has been plotted in Fig. 4a,b as a dashed line, and the intersection with the stress-strain curves as black squares. The slopes of the linear fits to the strain-temperature curves give the thermal expansion coefficient as a function of stress, which is plotted in Figure 4c. From this data, it is clear that increasing the temperature causes elongation of the graphene, which

is in contrast to prevailing expectations from membrane theory.[32] Furthermore, the thermal expansion coefficient increases linearly with tension, which is also surprising.

The same out-of-plane phonon modes that are predicted to cause the TEC to be negative are also expected to soften the in-plane stretching modulus with increasing temperature. This has been observed in lipid membrane experiments[33] and molecular dynamics (MD) simulations of graphene.[34] While our data does show a softening modulus with increasing temperature, it softens by a factor of ∼4-8 from 78 K to 297 K, while Ref. 34 predicts a factor of ∼1.4 over the same range. Hence, the magnitude of this effect is too large to be caused by thermal fluctuations alone. Similar to thermal ripples, static ripples would also soften the modulus, but they would not cause it to change with temperature.[35]

The incompatibility of the thermal membrane theory with our data suggests another, more dominant effect at play in graphene membranes, which causes the modulus to soften near room temperature and leads to a positive thermal expansion coefficient. In an attempt to understand this effect, we first note that a positive TEC follows directly from a softening modulus. The total strain of a tensioned membrane can be written as a combination of thermal and tensile contributions: $\epsilon(\sigma, T) = \epsilon(0, T) + \frac{\sigma}{E(T)}$, where $\epsilon(0, T)$ is the initial strain caused by a change in temperature, σ is the tension induced by external forces, such as a gate voltage, and $E(T)$ is the modulus. Hence, the thermal expansion coefficient at a fixed tension is given by:

$$\alpha = \left.\frac{\partial \epsilon(\sigma, T)}{\partial T}\right|_{\sigma} = \frac{\partial \epsilon(0, T)}{\partial T} - \frac{\sigma}{E(T)^2}\frac{\partial E(T)}{\partial T} \tag{2}$$

The first term above is the usual thermal expansion coefficient for untensioned graphene, while the second term accounts for nonzero tension and a temperature-dependent modulus. According to our experiment, $\partial E/\partial T$ is negative and large enough to dominate the bare thermal expansion. We measure a stress-dependent TEC of $\sim 30 \times 10^{-6}\mathrm{K}^{-1}$, which has opposite sign and is larger in magnitude than the theoretical TEC of graphene ($\sim -4 \times 10^{-6}\mathrm{K}^{-1}$).[16] Furthermore, the TEC of the silicon substrate is less than $\sim 2 \times 10^{-6}\mathrm{K}^{-1}$,[36] in the temperature range studied, which is also small compared to what we measure. Hence,

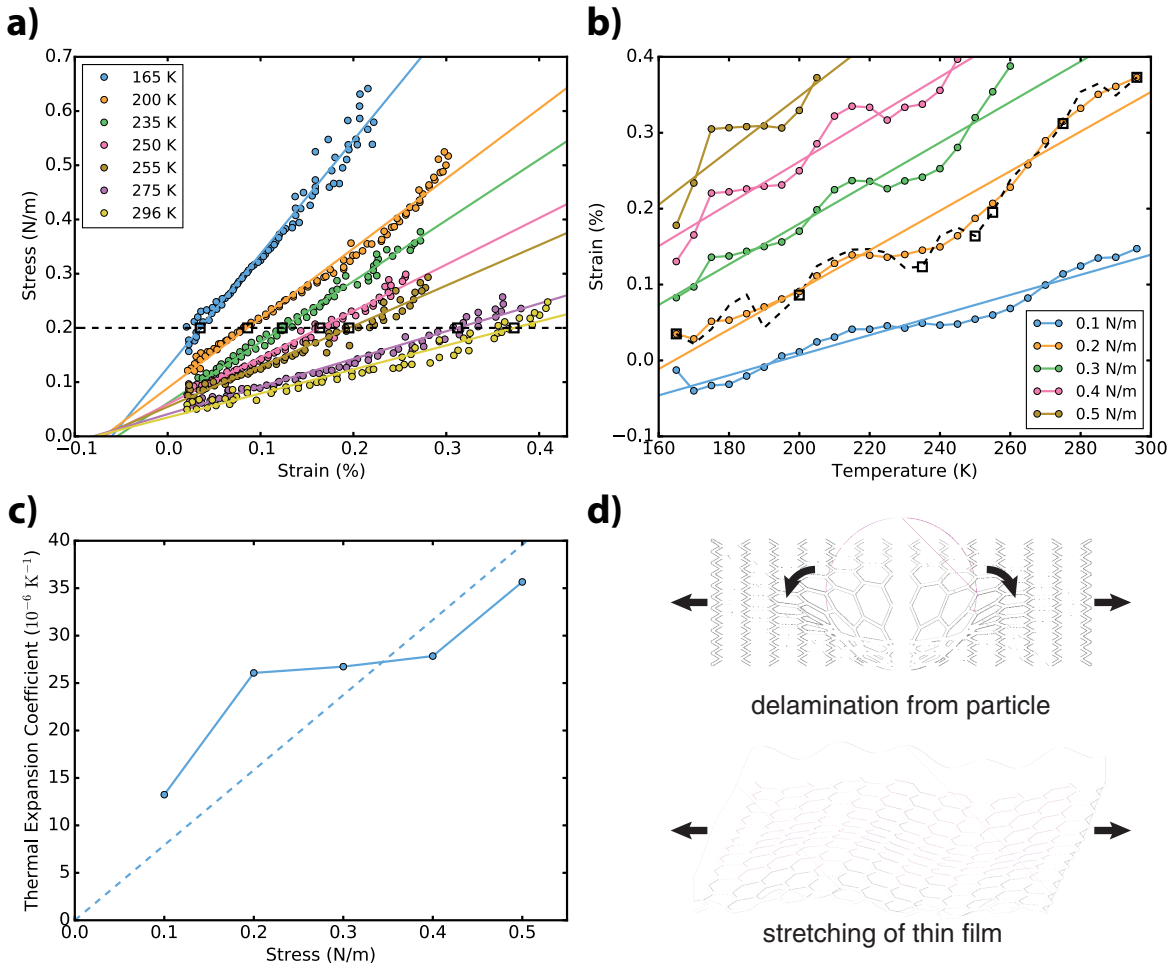

Figure 4: (a) Select stress-strain curves for Device 2, Run 1, derived from the force-distance data, with linear fits. The slopes of these lines show that the Young's modulus increases with decreasing temperature. (b) The same force-distance data plotted as induced strain versus temperature at fixed tensions, with linear fits. The data is smoothed using a 5-point square window, to pull out the trend. Note that these curves are correlated because they are taken at equally spaced intervals in stress and the modulus is essentially constant with respect to strain. The small deviations from the linear fit are due to variations in the measured modulus at different temperatures (Note the spread in Fig. 3b). The dashed line and black squares in (a) map onto those in (b). (c) The thermal expansion coefficient as a function of stress, from the slopes of the linear fits in (b). The dashed line is a linear fit to the data, pinned at the origin. (d) Schematic showing two possible interactions that a graphene sheet could have with surface contamination, which would give rise to an effective Young's modulus that is softer than that of bare graphene and a positive thermal expansion coefficient.

a temperature-dependent modulus leads to a positive thermal expansion coefficient. Note that in the standard theory for thermally fluctuating membranes, the first term dominates and the thermal expansion coefficient is negative.[32]

One obvious candidate for the source of this temperature-dependent modulus is polymeric contamination on the graphene membrane. Careful studies by transmission electron microscopy (TEM) and Raman spectroscopy have shown that 1-2 nm of PMMA is adsorbed on contact with graphene, which cannot be removed entirely by annealing.[26] Such contamination appears in resonance measurements as additional mass.[11,15] Because of its low bending stiffness and strong van der Waals bonding, graphene will adhere to any surface contaminants, creating effectively rippled graphene. Extension can then occur when the graphene either stretches the contaminant or delaminates from it, as illustrated in Fig. 4d. We thus expect the effective modulus of the system to be between that of ideal graphene and the modulus of the residue. The 3D Young's modulus of PMMA is 2-3 GPa at room temperature,[37] and if there is at worst a 1-2 nm film on the graphene surface, then the 2D modulus of the contaminant film would be 2-6 N/m. Our measured moduli lie between these values and the ideal graphene modulus of 340 N/m. Delamination may also contribute, but is likely not the dominant effect. If we assume that the adhesion energy between graphene and the contaminants is comparable to that of graphene and other surfaces, then delaminating from contaminant particles would require a force of $\sim 0.45\,\mathrm{N/m}$,[38] larger than the tensions applied here. Furthermore, the modulus of organic materials, such as PMMA, grows significantly stiffer with decreasing temperature,[37,39,40] in agreement with the observed behavior. Future experiments that can control the amount of contamination (e.g. through annealing and/or evaporation), and simultaneously measure the modulus and mass, using static and resonant measurements, can determine whether this conjecture is correct.

Our results have interesting implications for previous graphene resonator experiments. These experiments use the resonant frequency to measure the tension indirectly. Experiments from several different groups, including ours, have all seen the frequency increase with

decreasing temperature,[11,15,41] Chen *et al.* (2009) asserted that this is due to the contraction of suspended gold electrodes, which counteracts the expansion of graphene.[11] The results of the measurements reported here, on devices with no suspended metal, point to an alternative explanation: that the temperature dependence of the modulus causes the effective TEC of a tensioned graphene membrane to be positive, and that this temperature dependence arises from surface contaminants. This explanation is also applicable to Chen *et al.* (2009), whose temperature measurements were performed on a device with 6.4 times the mass of bare graphene, indicating the presence of contamination. Hence, we have conclusively shown that the TEC of graphene is positive under typical experimental conditions, resolving one of the long-standing mysteries in the graphene resonator community.

Note that the situation changes above room temperature. Other experiments have measured the TEC of graphene using SEM[17] and Raman spectroscopy[18] at elevated temperatures, and found a negative value. In separate experiments, we have observed that the frequency of graphene resonators increases with increasing temperature, with the turnaround point being somewhere near room temperature.[42] This is consistent with the known glass temperature of typical polymer residues (300 - 400 K);[39] above this temperature, the polymer flows and the TEC becomes that of bare graphene.

Finally, we examine the softened modulus of graphene in the context of previous AFM nano-indentation experiments.[3,5] These experiments apply a point load to the graphene and measure a modulus of 340 N/m. However, this disagrees with our optical measurements of the modulus, in which we apply a uniform load. To resolve this discrepancy, we have developed a novel technique for using an AFM in tapping mode to measure the force-distance curve of a graphene membrane under uniform load, and compare it to a point load measurement on the same device. Figure 5a shows a 3D plot of AFM height data from an integrated device experiencing a uniform electrostatic force from an applied gate voltage. In Fig. 5b, line scans are taken across the center of a device with a 2.3 µm radius as the gate voltage is stepped from 0 V to 70 V (the scanning direction is perpendicular to the trench). The

shape is roughly parabolic, as expected for a tensioned membrane under uniform load.[19,43] Taking a vertical cut through the center of the data in Fig. 5b gives the force-distance curve plotted in Fig. 5c. Fitting Eq. 1 to the data gives $\sigma_0 = 0.063$ N/m and $E = 32$ N/m, which is in reasonable agreement with our optical measurements.

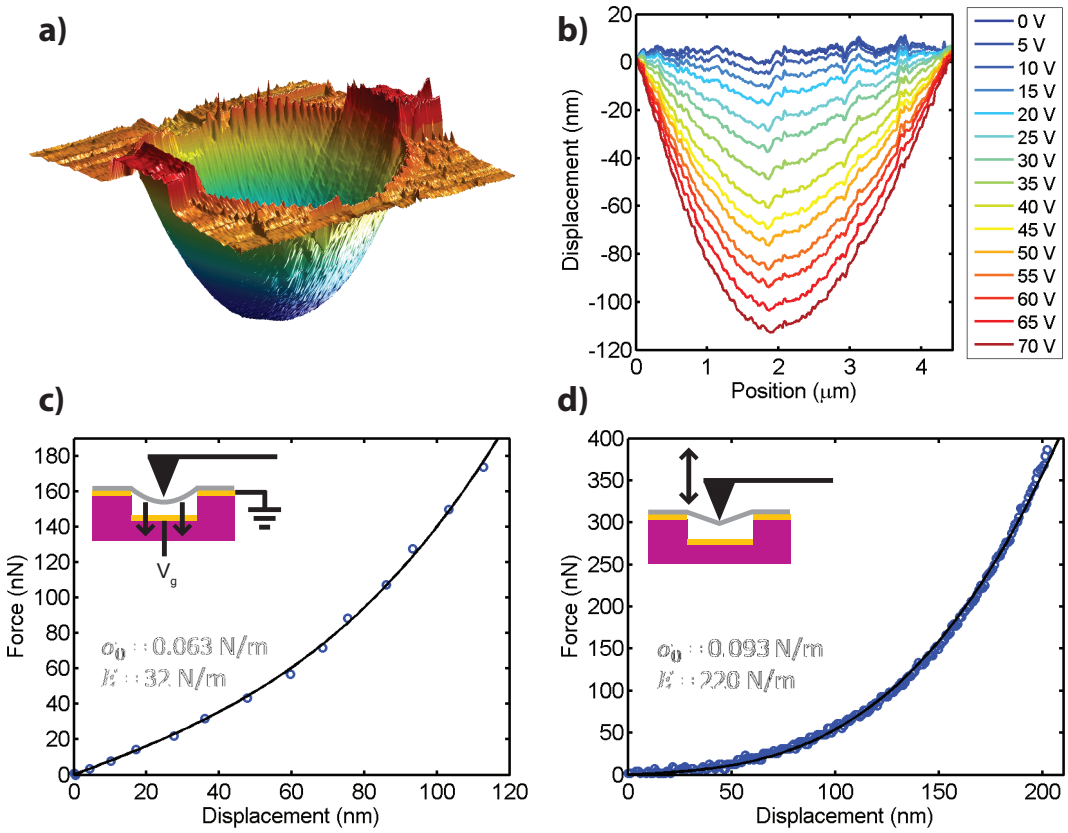

Figure 5: AFM measurements on graphene devices. (a) 3D reconstruction of AFM height image data for a typical graphene device experiencing a uniform force from an applied gate voltage. (b) Line cuts across the center of a 2.3 μm radius device showing how the profile changes as the gate voltage is varied. The AFM tip was grounded for these measurements. (c) Force-distance curve from a vertical line cut at ∼2 μm (center of the membrane), calculated assuming the force from a parallel plate capacitor model. The black line is a fit of Eq. 1 to the data. (d) Force-distance curve obtained by pushing with the AFM tip in the center of the same device. The black line is a fit of Eq. 3 to the data.

For comparison, we also performed nano-indentation measurements on the same device, in which the AFM tip itself is used to apply a point force while the tip deflection is measured.[44]

The deflection sensitivity is found by pressing the tip into a hard surface (the nearby silicon substrate), and the spring constant is determined by fitting a Lorentzian to the power spectral density of the thermal motion of the tip. The tip used for this measurement has a spring constant of ∼70 N/m. The resulting force-distance curve is plotted in Fig. 5d, and it is also well fit by linear and cubic terms. The theoretical force-distance curve for a tensioned membrane under point load is given by:[20,30,45]

$$F = \frac{2\pi}{\log R/r}\sigma_0 z + \frac{E}{f^3}\frac{z^3}{R^2} \tag{3}$$

where $f = 1.05 - 0.15\nu - 0.16\nu^2 = 1.02$ and r is the radius of the AFM tip. Assuming a typical AFM tip radius of ∼20 nm, a fit to the data gives $\sigma_0 = 0.093$ N/m and $E = 220$ N/m. This fit includes the asymmetric part of the curve at negative displacement (not plotted here) when the tip is retracted, in order to accurately determine the zero displacement point.

The two different load cases give similar values for the initial tension, but very different values for the Young's modulus. We do not have a conclusive explanation for this discrepancy, but one key difference between the two load cases is the distribution of the strain across the membrane. Under uniform load, the strain is uniformly distributed, but under point load, the strain is highly localized near the AFM tip. It is possible that such high strain causes the graphene to be fully stretched and exhibit a modulus closer to that of flat graphene (340 N/m). Future work, both theoretical and experimental, is needed to prove or disprove this conjecture. In any case, the fact that different load conditions produce a different value for the effective modulus has broader implications for graphene resonator and mass-sensing experiments that assume the modulus is equal to the theoretical value for flat graphene (340 N/m) inferred from point load experiments, even though the force is uniformly applied.[11]

In summary, we have used an optical technique for detecting the static displacement of a graphene membrane to measure force-distance curves at various temperatures. We find that the Young's modulus at room temperature is significantly softer than at low temperature.

This causes the thermal expansion coefficient to be positive for a tensioned membrane, which is contrary to expectations from the literature. We tentatively attribute this behavior to the effects of polymer residue on the graphene surface. Interestingly, we find that force-distance curves measured by AFM produce different results for point and uniform loads on the same membrane, which suggests that the commonly used modulus of 340 N/m is not appropriate for the analysis of graphene under electrostatic force.[11]

Acknowledgement

This work was supported in part by the Cornell Center for Materials Research with funding from the NSF MRSEC program (DMR-1120296), in part by the Institute for Nanoelectronics Discovery and Exploration, and in part by the AFOSR MURI. IRS acknowledges support from the NSF IGERT program (DGE-0903653). Sample fabrication was performed at the Cornell NanoScale Science and Technology Facility, a member of the National Nanofabrication Infrastructure Network, funded by the NSF. We also thank Jonathan Alden, Arthur Barnard, Alejandro Cortese, Andrej Kosmrlj, Kathryn McGill, David Nelson, Peter Rose, Eric Smith, and Natalia Storch for helpful discussions.

References

(1) Geim, A. K.; Novoselov, K. S. *Nat. Mater.* **2007**, *6*, 183–191.

(2) Bunch, J. S.; van der Zande, A. M.; Verbridge, S. S.; Frank, I. W.; Tanenbaum, D. M.; Parpia, J. M.; Craighead, H. G.; McEuen, P. L. *Science* **2007**, *315*, 490–493.

(3) Lee, C.; Wei, X.; Kysar, J. W.; Hone, J. *Science* **2008**, *321*, 385–388.

(4) Frank, I. W.; Tanenbaum, D. M.; van der Zande, A. M.; McEuen, P. L. *J. Vac. Sci. Technol. B* **2007**, *25*, 2558–2561.

(5) Lee, G.-H.; Cooper, R. C.; An, S. J.; Lee, S.; van der Zande, A. M.; Petrone, N.; Hammerberg, A. G.; Lee, C.; Crawford, B.; Oliver, W. *Science* **2013**, *340*, 1073–1076.

(6) Castellanos-Gomez, A.; Singh, V.; van der Zant, H. S. J.; Steele, G. A. *Ann. Phys.* **2015**, *527*, 27–44.

(7) Akinwande, D.; Brennan, C. J.; Bunch, J. S.; Egberts, P.; Felts, J. R.; Gao, H.; Huang, R.; Kim, J.; Li, T.; Li, Y. et al. *Extreme Mech. Lett.* **2017**, *13*, 42–77.

(8) Lpez-Poln, G.; Gmez-Navarro, C.; Parente, V.; Guinea, F.; Katsnelson, M. I.; Prez-Murano, F.; Gmez-Herrero, J. *Nat. Phys.* **2015**, *11*, 26–31.

(9) Lpez-Poln, G.; Jaafar, M.; Guinea, F.; Roldn, R.; Gmez-Navarro, C.; Gmez-Herrero, J. *Carbon* **2017**, *124*, 42–48.

(10) Barton, R. A.; Parpia, J.; Craighead, H. G. *J. Vac. Sci. Technol. B* **2011**, *29*, 050801.

(11) Chen, C.; Rosenblatt, S.; Bolotin, K. I.; Kalb, W.; Kim, P.; Kymissis, I.; Stormer, H. L.; Heinz, T. F.; Hone, J. *Nat. Nanotechnol.* **2009**, *4*, 861–867.

(12) Storch, I. R., Ph.D. thesis, Cornell University, 2015.

(13) Barton, R. A.; Storch, I. R.; Adiga, V. P.; Sakakibara, R.; Cipriany, B. R.; Ilic, B.; Wang, S. P.; Ong, P.; McEuen, P. L.; Parpia, J. M. et al. *Nano Lett.* **2012**, *12*, 4681–4686.

(14) Chen, C.; Lee, S.; Deshpande, V. V.; Lee, G.-H.; Lekas, M.; Shepard, K.; Hone, J. *Nat. Nanotechnol.* **2013**, *8*, 923–927.

(15) Singh, V.; Sengupta, S.; Solanki, H. S.; Dhall, R.; Allain, A.; Dhara, S.; Pant, P.; Deshmukh, M. M. *Nanotechnology* **2010**, *21*, 165204.

(16) Mounet, N.; Marzari, N. *Phys. Rev. B* **2005**, *71*, 205214.

(17) Bao, W.; Miao, F.; Chen, Z.; Zhang, H.; Jang, W.; Dames, C.; Lau, C. N. *Nat. Nanotechnol.* **2009**, *4*, 562–566.

(18) Yoon, D.; Son, Y.-W.; Cheong, H. *Nano Lett.* **2011**, *11*, 3227–3231.

(19) Timoshenko, S. *Theory of Elasticity*; McGraw-Hill, 1934.

(20) Komaragiri, U.; Begley, M. R.; Simmonds, J. G. *J. Appl. Mech.* **2005**, *72*, 203–212.

(21) Nicholl, R. J. T.; Conley, H. J.; Lavrik, N. V.; Vlassiouk, I.; Puzyrev, Y. S.; Sreenivas, V. P.; Pantelides, S. T.; Bolotin, K. I. *Nat. Commun.* **2015**, *6*, 8789.

(22) Li, X.; Cai, W.; An, J.; Kim, S.; Nah, J.; Yang, D.; Piner, R.; Velamakanni, A.; Jung, I.; Tutuc, E. et al. *Science* **2009**, *324*, 1312–1314.

(23) Barton, R. A.; Ilic, B.; van der Zande, A. M.; Whitney, W. S.; McEuen, P. L.; Parpia, J. M.; Craighead, H. G. *Nano Lett.* **2011**, *11*, 1232–1236.

(24) Adiga, V. P.; De Alba, R.; Storch, I. R.; Yu, P. A.; Ilic, B.; Barton, R. A.; Lee, S.; Hone, J.; McEuen, P. L.; Parpia, J. M. et al. *Appl. Phys. Lett.* **2013**, *103*, 143103.

(25) Bolotin, K. I.; Sikes, K. J.; Jiang, Z.; Klima, M.; Fudenberg, G.; Hone, J.; Kim, P.; Stormer, H. L. *Solid State Commun.* **2008**, *146*, 351–355.

(26) Lin, Y.-C.; Lu, C.-C.; Yeh, C.-H.; Jin, C.; Suenaga, K.; Chiu, P.-W. *Nano Lett.* **2012**, *12*, 414–419.

(27) Cartamil-Bueno, S. J.; Steeneken, P. G.; Centeno, A.; Zurutuza, A.; van der Zant, H. S. J.; Houri, S. *Nano Lett.* **2016**, *16*, 6792–6796.

(28) Bao, W.; Myhro, K.; Zhao, Z.; Chen, Z.; Jang, W.; Jing, L.; Miao, F.; Zhang, H.; Dames, C.; Lau, C. N. *Nano Lett.* **2012**, *12*, 5470–5474.

(29) Nair, R. R.; Blake, P.; Grigorenko, A. N.; Novoselov, K. S.; Booth, T. J.; Stauber, T.; Peres, N. M. R.; Geim, A. K. *Science* **2008**, *320*, 1308–1308.

(30) Wan, K.-T.; Guo, S.; Dillard, D. A. *Thin Solid Films* **2003**, *425*, 150–162.

(31) Kudin, K. N.; Scuseria, G. E.; Yakobson, B. I. *Phys. Rev. B* **2001**, *64*, 235406.

(32) Nelson, D.; Weinberg, S.; Piran, T. *Statistical Mechanics of Membranes and Surfaces*; Wspc, 2004.

(33) Evans, E.; Rawicz, W. *Phys. Rev. Lett.* **1990**, *64*, 2094–2097.

(34) Gao, W.; Huang, R. *J. Mech. Phys. Solids* **2014**, *66*, 42–58.

(35) Košmrlj, A.; Nelson, D. R. *Phys. Rev. E* **2013**, *88*, 012136.

(36) Okada, Y.; Tokumaru, Y. *J. Appl. Phys.* **1984**, *56*, 314–320.

(37) Imai, Y.; Brown, N. *J. Mater. Sci.* **1976**, *11*, 417–424.

(38) Koenig, S. P.; Boddeti, N. G.; Dunn, M. L.; Bunch, J. S. *Nat. Nanotechnol.* **2011**, *6*, 543–546.

(39) Ao, Z.; Li, S. *Nanoscale Res. Lett.* **2011**, *6*, 1–6.

(40) Imai, Y.; Brown, N. *Polymer* **1977**, *18*, 298–304.

(41) van der Zande, A. M.; Barton, R. A.; Alden, J. S.; Ruiz-Vargas, C. S.; Whitney, W. S.; Pham, P. H. Q.; Park, J.; Parpia, J. M.; Craighead, H. G.; McEuen, P. L. *Nano Lett.* **2010**, *10*, 4869–4873.

(42) De Alba, R.; Abhilash, T. S.; Hui, A.; Storch, I. R.; Craighead, H. G.; Parpia, J. M. *J. Appl. Phys.* **2018**, *123*, 095109.

(43) Timoshenko, S.; Woinowsky-Krieger, S. *Theory of plates and shells*; McGraw-Hill, 1959.

(44) Whittaker, J. D.; Minot, E. D.; Tanenbaum, D. M.; McEuen, P. L.; Davis, R. C. *Nano Lett.* **2006**, *6*, 953–957.

(45) Vella, D.; Davidovitch, B. *Soft Matter* **2017**, *13*, 2264–2278.